Chemical Science

EDGE ARTICLE

View Article Online
View Journal | View Issue

Cite this: *Chem. Sci.*, 2019, **10**, 4107

All publication charges for this article have been paid for by the Royal Society of Chemistry

Proline bulky substituents consecutively act as steric hindrances and directing groups in a Michael/Conia-ene cascade reaction under synergistic catalysis†

Salil Putatunda, ‡[a] Juan V. Alegre-Requena, ‡[b] Marta Meazza, [c] Michael Franc, [a] Dominika Rohal'ová,[a] Pooja Vemuri,[c] Ivana Císařová, [d] Raquel P. Herrera, *[b] Ramon Rios *[c] and Jan Veselý *[a]

In this study, we report a highly stereoselective and versatile synthesis of spiro pyrazolones, promising motifs that are being employed as pharmacophores. The new synthetic strategy merges organocatalysis and metal catalysis to create a synergistic catalysis using proline derivatives and Pd catalysts. This protocol is suitable for late-stage functionalization, which is very important in drug discovery. Additionally, a thorough computational study proved to be very useful to elucidate the function of the different catalysts along the reaction, showing a peculiar feature: the $-CPh_2OSiMe_3$ group of the proline catalyst switches its role during the reaction. In the initial Michael reaction, this group plays its commonly-assumed role of bulky blocking group, but the same group generates π–Pd interactions and acts as a directing group in the subsequent Pd-catalyzed Conia-ene reaction. This finding might be very relevant especially for processes with many steps, such as cascade reactions, in which functional groups are assumed to play the same role during all reaction steps.

Received 26th November 2018
Accepted 3rd March 2019

DOI: 10.1039/c8sc05258a

rsc.li/chemical-science

Introduction

The synthesis of highly complex scaffolds has long generated considerable research interest among organic chemists. Some of the most challenging organic structures to synthesize are spiro compounds (formally bicyclic organic compounds with rings connected through a quaternary atom centre).[1–8] Spirocycles have unique structural properties due to their rigidity, and they are present in several natural products such as spongistatins, fredericamycin, the fused tetracyclic lycopodium alkaloid nankakurine A (**1**) and alkaloid (−)-sibirine (**2**), and in pharmaceuticals (Fig. 1).[9,10] However, libraries of spiro compounds are still underrepresented in medicinal chemistry despite their usefulness as rigid conformations that reduce conformational entropy penalty when binding to pharmaceutical targets.[9,10] Recent advances in synthetic methods have provided access to spiro building blocks, thereby slightly expanding their use in drug discovery. However, further synthetic work is clearly still needed because spirocycles are difficult to prepare. Their synthesis involves the formation of a quaternary center, which is a challenging task in synthetic organic chemistry.

Recently, we have focused our efforts on developing enantioselective methods for the synthesis of spiro compounds through organocatalytic cascade reactions,[11,12] using a synergistic approach.[13] It is remarkable that synergistic catalysis has opened an exciting gate for the development of new reactions due to the possibility to activate two unreactive compounds at the same time.[14,15]

Pyrazolones are a key class of five-membered ring nitrogen heterocycles, which have been used as pharmaceutical agents,

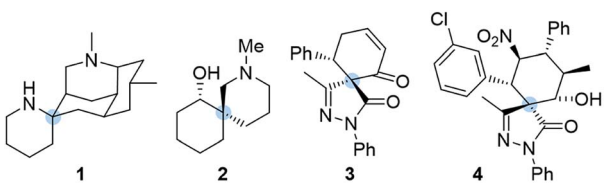

Fig. 1 Spirocyclic natural products and pharmacophores.

[a]*Department of Organic Chemistry, Faculty of Science, Charles University, Hlavova 2030, 128 43 Praha 2, Czech Republic. E-mail: jxvesely@natur.cuni.cz*

[b]*Laboratorio de Organocatálisis Asimétrica, Departamento de Química Orgánica, Instituto de Síntesis Química y Catálisis Homogénea (ISQCH), CSIC-Universidad de Zaragoza, C/Pedro Cerbuna 12, 50009 Zaragoza, Spain. E-mail: raquelph@unizar.es*

[c]*University of Southampton, School of Chemistry, Highfield Campus, Southampton, SO17 1BJ, UK. E-mail: rrt1f11@soton.ac.uk*

[d]*Department of Inorganic Chemistry, Faculty of Science, Charles University, Hlavova 2030, 128 43 Praha 2, Czech Republic*

† Electronic supplementary information (ESI) available. CCDC 1859005 and 1859006. For ESI and crystallographic data in CIF or other electronic format see DOI: 10.1039/c8sc05258a

‡ These authors contributed equally to this work.

agrochemicals, and chelating agents, among others.[16,17] Pyrazole units are found in many natural products such as withasonine, pyrazofurin and formicin. Moreover, their use in pharmaceutical chemistry has increased due to their properties as p38 inhibitors and HIV integrase inhibitors.[18] More specifically, spiro pyrazolones have been used as promising pharmacophores, showing potential as antitumor (**3**) and anti-inflammatory (**4**) agents (Fig. 1).[19–22] In our research group, we have investigated the synthesis of spiropyrazolones by organocatalytic procedures (Scheme 1)[23,24] and very recently by a synergistic approach.[25]

To combine spiropyrazolone synthesis with synergistic catalysis, we focused on the venerable Conia-ene reaction as a viable synthetic tool to build five-membered (hetero) carbocycles.[26,27] Previously, the Cordova's group developed a Conia-ene reaction to prepare spirooxindoles with excellent results[28,29] and, more recently, Enders and colleagues reported the synthesis of spiropyrazolones by sequential organo- and silver catalysis.[30,31] The latter involves a Michael/Conia-ene cascade reaction between pyrazolones and nitroalkenes bearing an alkyne (Scheme 1).

Inspired by these results, we envisioned a completely new strategy involving alkyne tethered pyrazolones **5** and enals **6** (Scheme 2). First, proline derived catalysts would be used to achieve a highly stereoselective activation of enals. Another reason to use this type of catalyst is that they preserve their catalytic activity even when metal Lewis acids, such as Pd, In and Ag, are also present in the reaction media.[32–34] Moreover, we considered that this method could be easily applied to generate broad libraries of spiro compounds because enals **6** and pyrazolones **5** are easily synthesized and functionalized, and the compounds generated **7** contain several reactive groups (aldehydes, double bonds), thus enabling late-stage functionalization.

Moreover, the concurrent activation of both reactants through a synergistic catalysis allows a major reactivity scope and, at the same time, the use of simple catalysts that are not interconnected (in opposition to bifunctional catalysts[35–37]) (Fig. 2). Additionally, these processes require less synthetic effort in the reaction optimization process because each catalyst can be individually optimized.

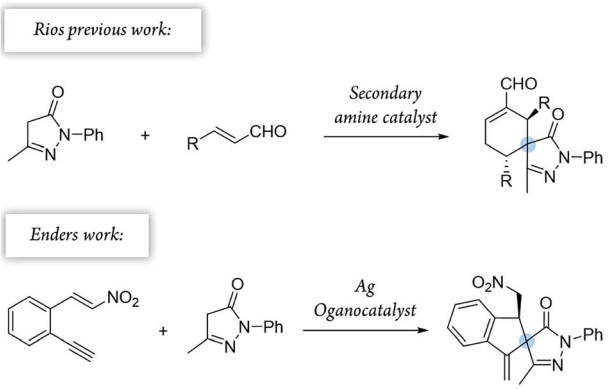

Scheme 1 Previously developed Michael/Conia-ene cascade reactions.

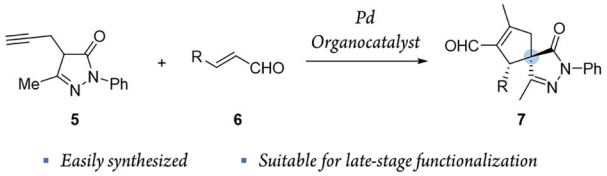

Scheme 2 New synergistic catalysis developed in this study to generate spiro pyrazolones **7**.

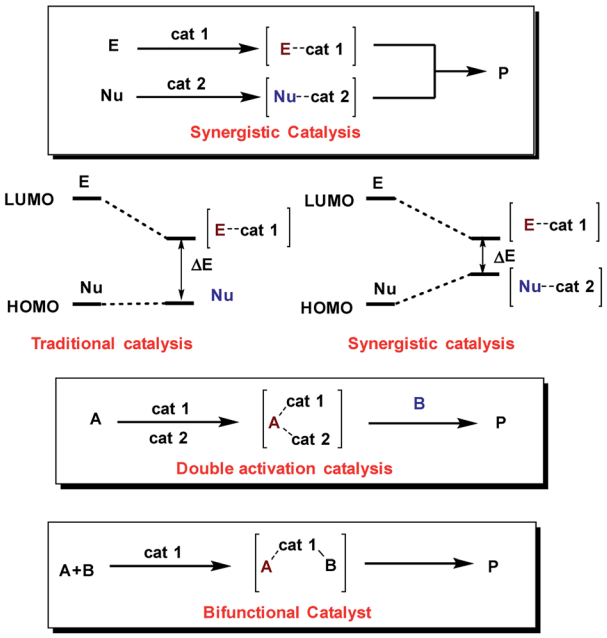

Fig. 2 Synergistic catalysis against traditional and bifunctional catalysis.

Results and discussion

Synthetic results

After optimizing the model reaction, we achieved our best results when using ethyl acetate as the solvent, at room temperature, in the presence of 5 mol% TMS-protected diphenyl prolinol (**I**), acting as the secondary amine catalyst, and 2 mol% $Pd_2(dba)_3$ (see the ESI† for more details about the optimization process). Remarkably, the reaction is catalyzed with a low organocatalyst loading (5 mol%), in contrast to similar organocatalytic reactions normally requiring 20 mol% of (**I**). Moreover, without adding Pd, no cyclization reaction is detected, highlighting the importance of this synergistic cascade.

Thus, we studied the scope of this reaction using several enals **6** to demonstrate the general applicability of this synergistic cascade reaction (Scheme 3).

In general, good-to-excellent yields of spiro compounds **7** with excellent enantioselectivities and moderate-to-good

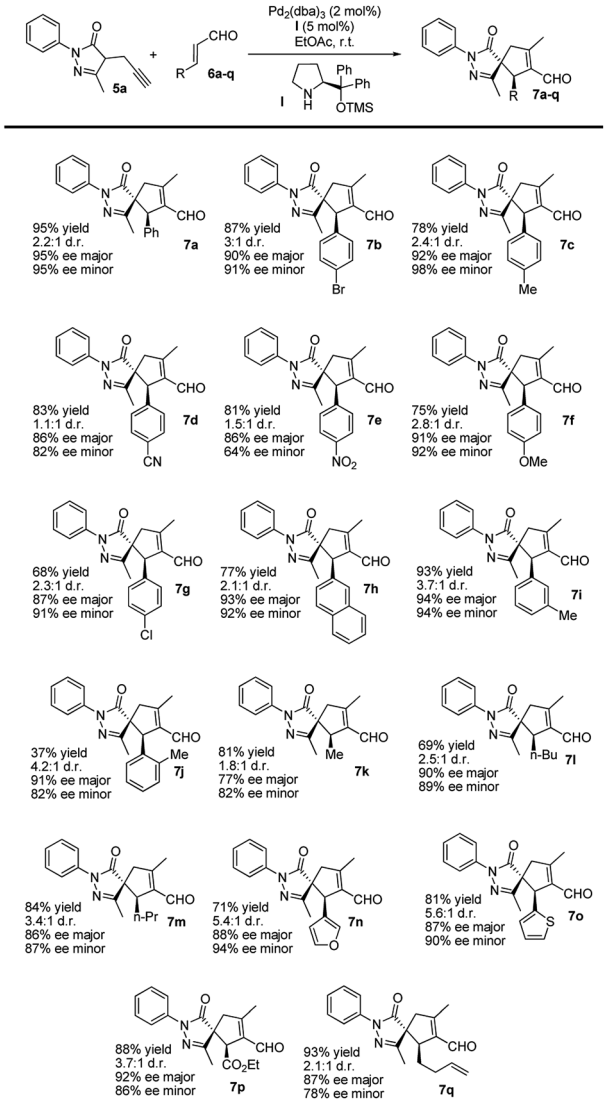

Scheme 3 Michael/Conia-ene cascade reaction between pyrazolone **5a** and enals **6a–q**.

diastereoselectivities were assessed with different enals. The reaction is compatible with aliphatic enals (**7k**, **7l** and **7m**), with the glyoxylate derivative (**7p**), with dienals (**7q**), with aromatic enals with electron withdrawing groups (**7d**, **7e**) and with electron donating groups (**7c**, **7f**) in a *para* position on the aromatic ring. Moreover, *meta*-substituted aromatic enal (**7i**) and heteroaromatic enals (**7n** and **7o**) were prepared in excellent yields. As a general trend, heteroaromatics render final compounds **7** in higher diastereoselectivities (up to 5.6 : 1 dr) whereas spiro compound **7j** was formed in low yields when using the *ortho*-substituted cinnamic-type enal, most likely for steric reasons.

Subsequently, we studied the process using substituted pyrazolones **5b–i** (Scheme 4). The reaction is sensitive to steric effects of the pyrazolones. When the initial Me group on the pyrazolone moiety was changed to a Ph group, the reaction rate significantly decreased. No full conversion was observed, even after a prolonged time (7 days), thus forming the corresponding

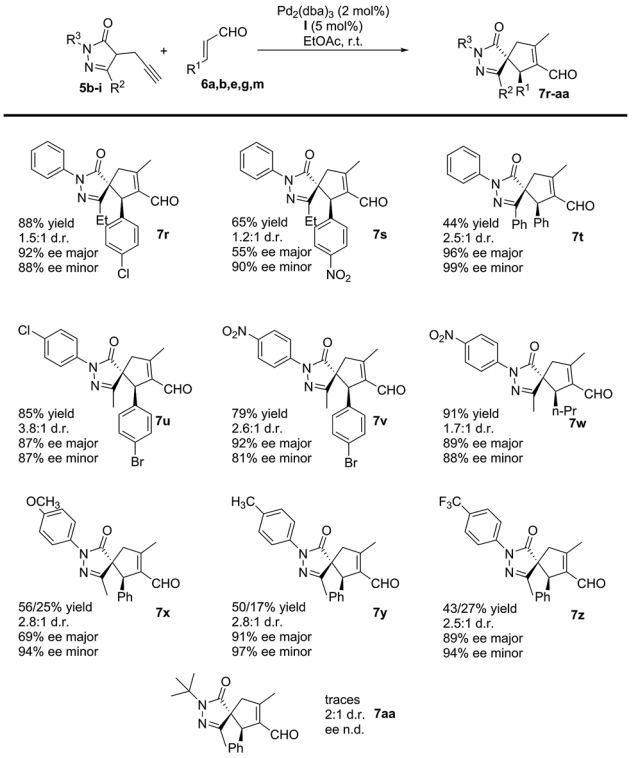

Scheme 4 Michael/Conia-ene reaction between pyrazolones **5b–i** and enals **6a,b,e,g,m**.

product **7t** in low yields. In contrast, when Et substituted pyrazolones were used, the results were similar to previously reported values when using their Me-substituted analogues (**7r** *vs.* **7g** and **7s** *vs.* **7e**). We finally studied the effect of different R^3 substituents: the reaction works well with EWG, EDG and halogen as 4-substituent of the aromatic ring (**7u–z**), while negligible conversion was observed when R^3 is an aliphatic substituent (**7aa**).

The absolute configuration of the final products was determined by X-ray diffraction analysis of compounds **8b** and **8b'** resulting from the oxidation of the separated diastereoisomers of **7b** (Fig. 3).[38] Based on the absolute configuration of the major diastereomer **8b**, intermediate **Int-Ald** contains two stereocenters that will be referred to as (*S*,*R*) in the computational study.

The versatility of the developed reaction has been demonstrated by late-stage derivatization of spiro compound **7b** (Scheme 5). Reduction and reductive amination of **7b**, used as a single diastereomer, afforded the corresponding alcohol **9b** and amine **10b**, respectively, in good yields, without losing enantiomeric purity. Similar result was found in Suzuki coupling with 4-methoxy phenyl boronic acid, affording spiro compound **11b**, containing a biphenyl motif.

Mechanistic studies

Initial experimental kinetic studies. Before designing the computational study of this reaction,[39–41] different experiments were performed to collect data on mechanistic parameters of this

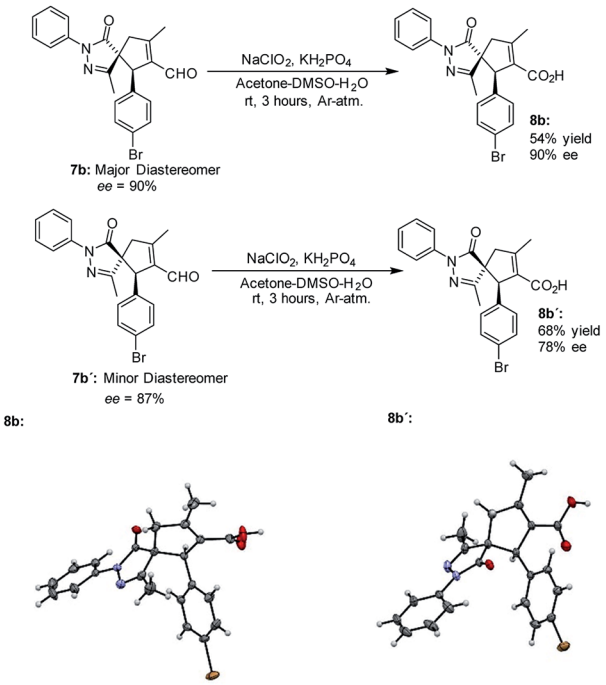

Fig. 3 Synthesis and X-ray structure of **8b** and **8b′**.

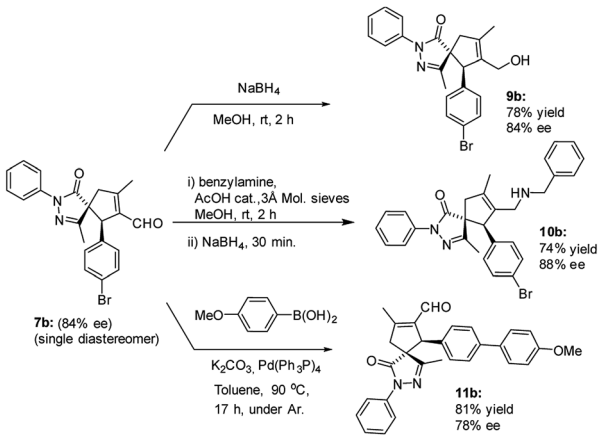

Scheme 5 Subsequent derivatizations of spiro compound **7b**.

process. Reaction kinetics assessed when using different amounts of the proline (**I**) and Pd catalysts were studied by NMR spectroscopy. These experiments were carefully performed to achieve significant results because most of the Pd catalysts are not soluble in the reaction media (see the ESI† for experimental details).

Additionally, we analyzed whether different parts of the reaction were reversible. The reaction was divided in two parts based on the two different C–C bond forming reactions (**TS-I** and **TS-II**) that occur during the whole process: part 1, including the Michael addition reaction that produces intermediate **Int-Ald**; and part 2, including the final Conia-ene reaction that generates product **7a** (Scheme 6).

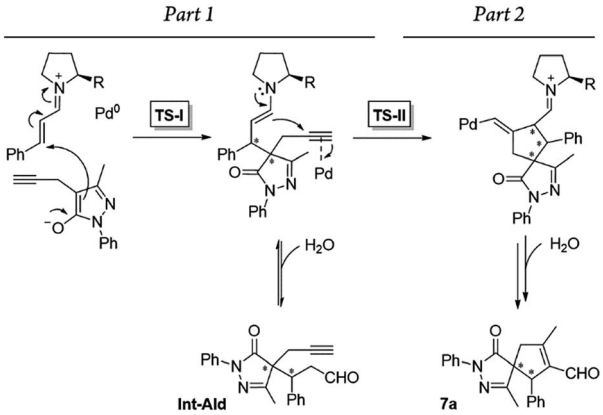

Scheme 6 Summary of the reaction steps of this cascade reaction divided into two parts based on the different C–C bond-forming reactions.

To study the reversibility of the different parts of the reaction, several variable temperature NMR experiments were conducted. In the first experiment, the reaction was performed without adding the Pd catalyst, and the Michael reaction (part 1) stopped before the initial reagents were completely consumed. When the reaction stopped (at 62% of cinnamaldehyde conversion, entry 1), we changed the temperature of the reaction mixture and analyzed how temperature variations affected the conversion (percentage) and diastereomeric ratio (dr) of intermediate **Int-Ald** (Table 1, entries 1–5 and Fig. S3†).

The results indicated that changes in temperature affected both conversion and dr. Interestingly, the variations in these parameters were reversible because, when the reaction was cooled down from 328 K to rt, the initial conversion and dr were observed again within 5–10 minutes (Table 1, entry 5). Furthermore, when pyrrolidine was used as the catalyst, the same dr was observed at rt although this catalyst is not chiral (Table 1, entries 1 and 6). These results suggest that this

Table 1 Conversion of cinnamaldehyde (**6a**) in the Michael (entries 1–6) and cascade reaction (entries 7–11) and dr of intermediate **Int-Ald** or product **7a** at different temperatures

Entry[a]	Substrate	T (K)	dr	Conversion (%)
1	**Int-Ald**	298	1 : 3.4	62
2	**Int-Ald**	308	1 : 3.3	55
3	**Int-Ald**	318	1 : 3.1	46
4	**Int-Ald**	328	1 : 2.9	40
5[b]	**Int-Ald**	298	1 : 3.4	62
6[c]	**Int-Ald**	298	1 : 3.4	—
7	**7a**	298	1 : 6.1	100
8	**7a**	308	1 : 6.0	100
9	**7a**	318	1 : 6.1	100
10	**7a**	328	1 : 6.0	100
11[c]	**7a**	298	1 : 1.5	—

[a] See the ESI for the reaction conditions of the kinetic experiments. [b] After cooling down the reaction from 328 K to 298 K. [c] Using pyrrolidine as the catalyst.

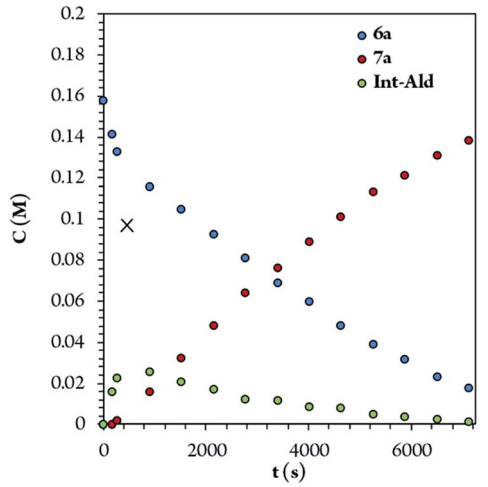

Fig. 4 Concentration of the different reaction components over time.

Michael reaction is reversible and that the conversion and dr are primarily determined by the energy of the different diastereomers of **Int-Ald** (thermodynamically controlled stereoselectivity)[41] rather than the energy of the transition states of C–C bond formation (**TS-I**, kinetically controlled stereoselectivity).

Similarly, we performed variable temperature NMR experiments using reactions containing both catalysts (**I** and Pd) and, therefore, leading to product **7a** (Table 1, entries 7–10). In contrast to the previous experiments, we observed no retro-Conia-ene reaction or variations in the dr of product **7a** at any temperature tested (Table 1 and Fig. S4†). Moreover, when pyrrolidine was used as the catalyst at rt, the dr of the product showed a significant change in comparison with the corresponding chiral reaction (Table 1, entries 7 and 11). These two findings suggest that the second part of the overall process is irreversible at the range of temperatures tested, thus indicating a Curtin–Hammett scenario (kinetically controlled stereoselectivity).[42]

To identify the rate- and enantio-determining steps, we analyzed the concentration profiles of the different reaction components. As previously observed, when the equilibrium of part 1 is reached, cinnamaldehyde (**6a**) conversion is 62%, and intermediate **Int-Ald** has an equilibrium concentration of 0.098 M (marked with an "*X*" next to the *Y* axis). Fig. 4 shows that intermediate **Int-Ald** reacts quickly and generates product **7a** before reaching the equilibrium concentration. This suggests that the slowest part of the reaction is part 1.

Although the stereocenters of the reactions are formed in part 1, diastereoselectivity changes from the intermediate **Int-Ald**, formed in part 1, to the final product **7a**, formed in part 2. The results from the kinetic studies suggest that (1) part 1 is slower than part 2 and that (2) the diastereoselectivity of the final product is determined in part 2. Thus, although part 1 contains the rate-limiting step (or steps), part 2 contains the stereo-determining step because the reactions of part 1 are reversible whereas at least one reaction of part 2 is irreversible. Accordingly, we designed a catalytic cycle based on all the data gathered in the kinetic studies (Scheme 7).

Computational study[43]

After the initial kinetic experiments, the reaction mechanism was computationally studied. All the calculations were

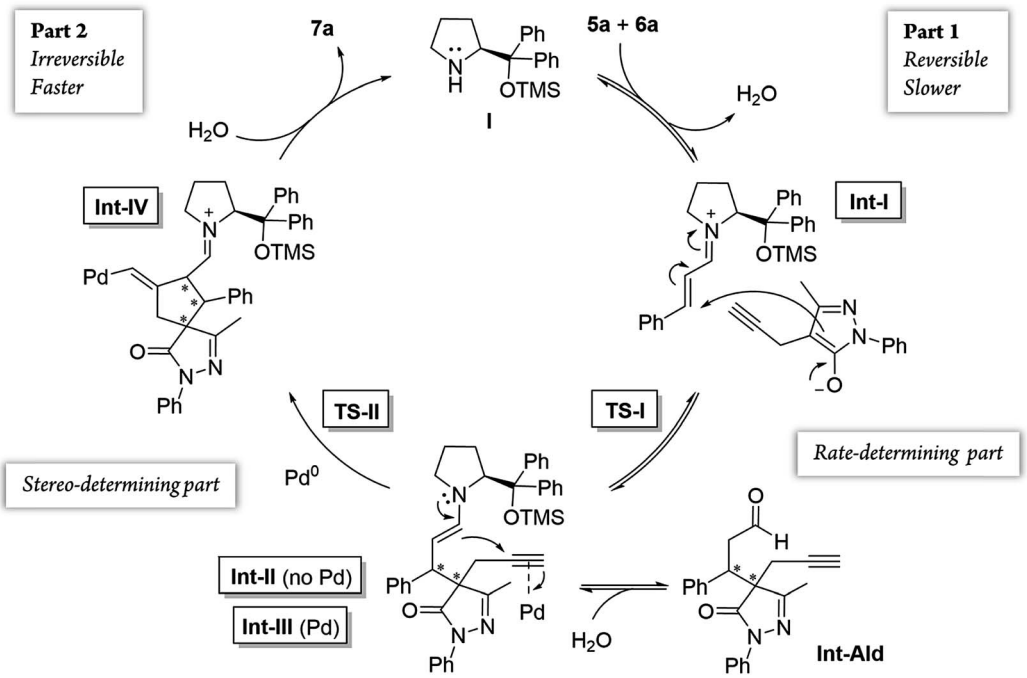

Scheme 7 General catalytic cycle of the cascade reaction studied.

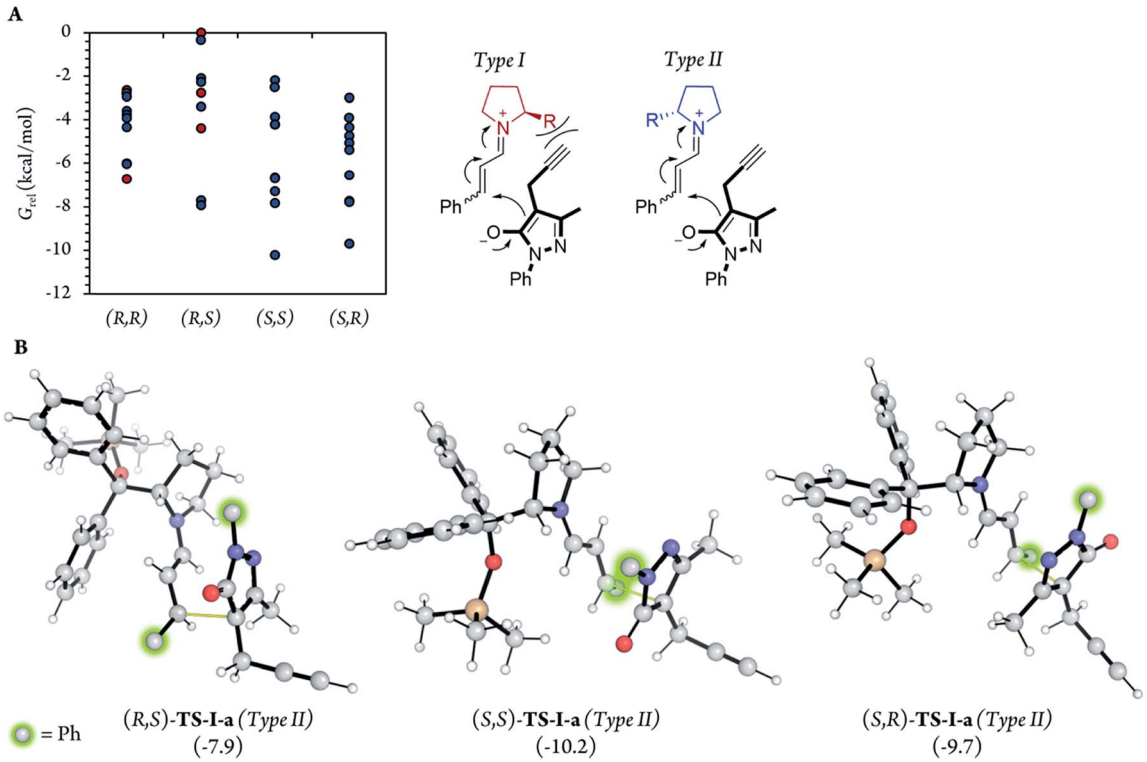

Fig. 5 (A) Relative *G* of the 10 most stable conformations of the **TS-I** step of each diastereoisomer, using the same point (least stable conformer, (*R*,*S*)-**TS-I-j**) as the reference in all cases and in different types of attack. Dots represent the energies of the different individual conformations. (B) Images of the most relevant **TS-I** steps, showing the C–C bond formation coordinates with thin yellow lines. 54 different conformations were analyzed for each diastereomer (216 conformations in total).

performed at the ωB97X-D/Def2-QZVPP(SMD)(UFgrid)//ωB97X-D/6-311G(d)(SMD)(UF grid) level (using the Def2-TZVP basis set for Pd atoms instead of the 6-311G(d) basis set in geometry optimizations). ωB97X-D is a highly reliable functional in similar reactions with many noncovalent interactions.[44–46] Moreover, we tested the validity of this computational approach in generating reliable structures by optimizing, using ωB97X-D/6-311G(d)(SMD)(UF grid), the geometry of a X-ray structure of

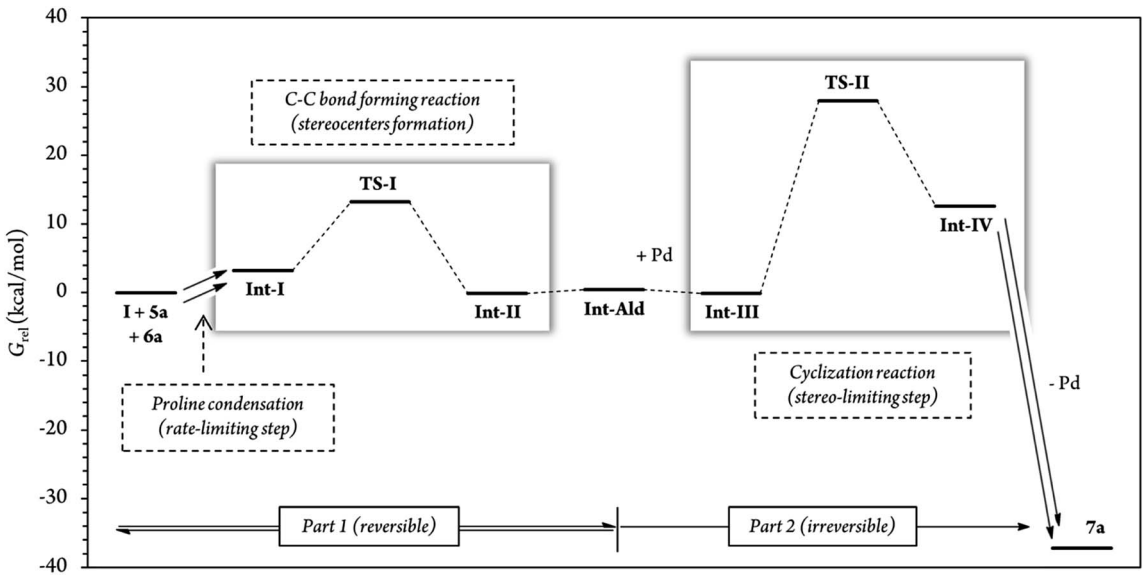

Fig. 6 Relative Gibbs free energies along the (*S*,*R*) reaction coordinate (for more information see section *G of the Calculations* of the ESI†). For this energy profile, we used Boltzmann average *G* of the 10 most stable conformations of each reaction step. A total of 54 different conformations were analyzed for steps **Int-I**, **TS-I** and **Int-II**, and 62 conformations for steps **Int-III**, **TS-II** and **Int-IV**.

the condensation product of proline (**I**) and cinnamaldehyde (**6a**).[47] In this analysis, we found no significant structural differences between the computationally optimized structure and its corresponding crystal structure (see the ESI† for more information). First, the energies of the first C–C bond forming step (**TS-I**) were calculated (Fig. 5). As explained above, even though the stereocenters are formed in this step (**TS-I**), this transition state does not determine the final stereoselectivity (*S*,*R*) of product **7a**. From the previous experiments, three important aspects of part 1 can be remarked: this part proceeds even when Pd is not added to the reaction; there is much more proline (**I**) in the reaction media than Pd; and the reaction rate does not vary in a great extent when Pd is added. Therefore, we can assume that most of the reaction pathways of part 1 and, therefore, most of the **TS-I** steps probably proceed without the Pd atom.

Although no information on the stereoselectivity of final product **7a** can be extracted from this study, a few common trends were observed among the most favorable **TS-I** steps of all diastereomers. Most importantly, the most stable **TS-I** steps lead to Michael reactions that occur on the opposite side of the proline substituent (–CPh_2OTMS), as previously proposed by other authors (Fig. 5A, Type II attack).[48] Furthermore, no significant noncovalent interactions occur between this group of the catalyst and the attacking pyrazolone group (**5a**). Therefore, the –CPh_2OTMS group of the proline sterically hinders the approach of **5a** to the side of the proline in which this blocking group is located.[47]

In addition, for further insight into the two C–C bond forming reactions (Fig. 6), we calculated Boltzmann averaged energies of the **Int-I**, **Int-II**, **Int-III**, **TS-II** and **Int-IV** systems of the (*S*,*R*) diastereomer, the major diastereomer of product **7a** observed experimentally. Using Boltzmann averaged energies of the different reaction coordinates is a useful strategy that has been previously applied to study the global mechanism of systems with multiple possible conformations.[49]

The calculations predicted that the *G* necessary to promote the retro-Michael reaction of part 1 (from aldehyde **Int-Ald** to **TS-I**) is much lower than that required for the retro-Conia-ene reaction of part 2 (from final product **7a** to **TS-II**). In fact, the

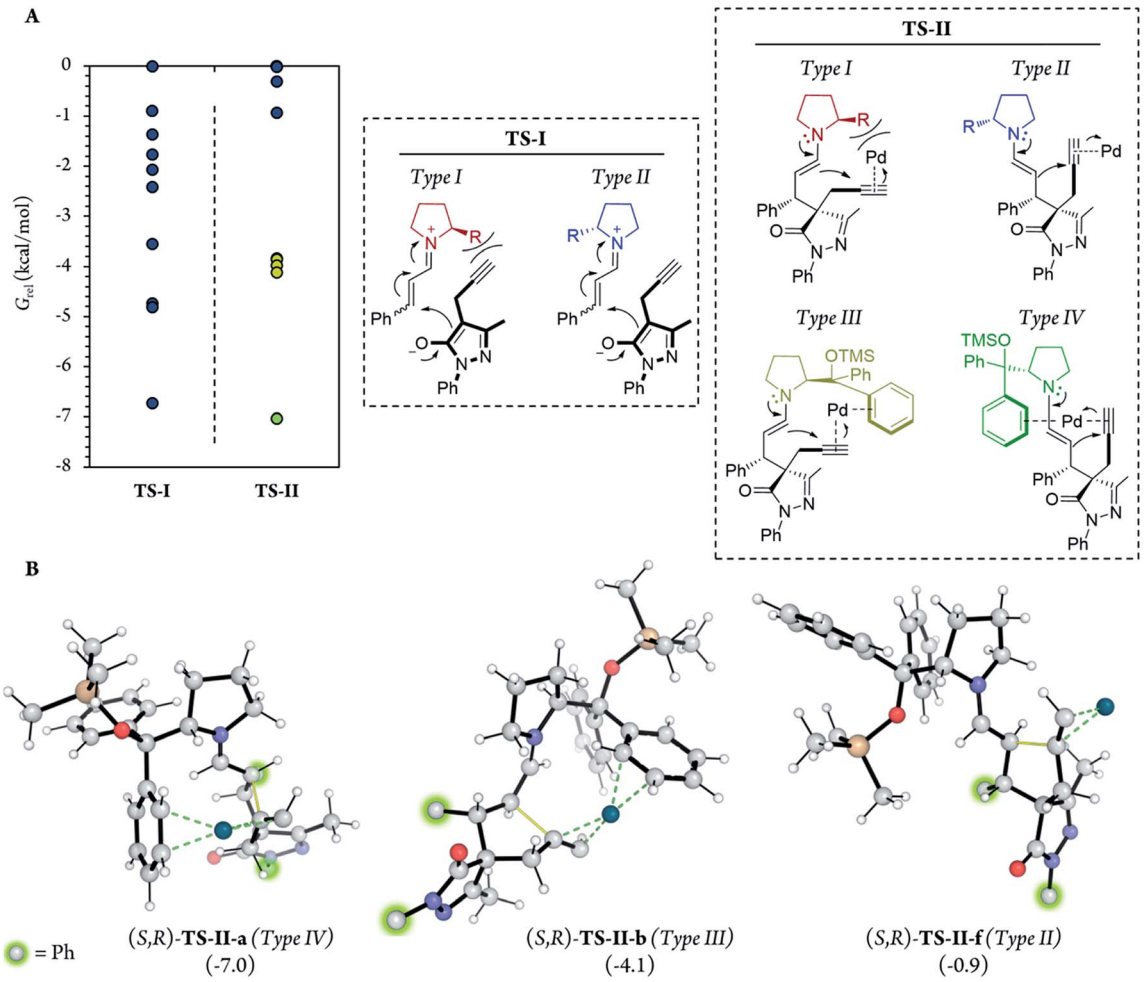

Fig. 7 (A) Energies of the (*S*,*R*)-TS-I and (*S*,*R*)-TS-II step along with the different types of attack in each transition state. Dots represent the relative energies of the 10 most stable conformations using the least stable conformers (TS-I-j and TS-II-j, respectively) as the reference for TS-I and TS-II. (B) Representation of the most favourable TS-II step of attack types II to IV (TS-II-a, TS-II-b and TS-II-f), showing C–C bond formation coordinates with thin yellow lines and π–Pd interactions with dashed green lines.

retro-Conia-ene reaction shows an activation G of 65.2 kcal mol^{-1}, which suggests that this retro-cyclization process is extremely slow at rt. This is in line with the initial experimental findings suggesting that part 1 is reversible, whereas part 2 is irreversible.

The experimental results showed that the rate-limiting step was enclosed in part 1 of the mechanism; however, the reaction coordinates from the computational study indicated that step **TS-II** (cyclization step), from part 2, had a much higher energy than **TS-I** (Michael addition). This difference suggests that the rate-limiting step is included in the initial iminium formation prior to the Michael reaction which agrees with the study conducted by Moliner, Luk and colleagues. These authors showed a relatively high G activation barrier of approximately 28 kcal mol^{-1} in the iminium formation between a proline derivative and cinnamaldehyde of a Henry reaction in various solvents.[50] Additionally, when we followed the reaction by ^{1}H-NMR experiments, we could not detect condensation products from catalyst (**I**) and cinnamaldehyde **6a**, that is, iminium ion intermediate is neither accumulated nor detected before the Michael addition (Fig. S5 and S6†). This strongly suggests that the subsequent step, the Michael addition reaction, is faster than the initial proline condensation with cinnamaldehyde **6a**. Thus, the *in situ* generated iminium ion intermediate would be rapidly consumed in the next step and consequently, not detected by NMR. Therefore, the NMR results from this study (Fig. 4 and S5, S6†) are in line with the computational energy profile calculated and indicate that the initial prolinol condensation with cinnamaldehyde **6a** is the rate-limiting step of the process.

Notably, in the most favorable **TS-II** step, the CPh_2OTMS group of proline (**I**) acts as a directing group due to a favorable π–Pd interaction (Fig. 7, *Type III* and *IV*), whereas this substituent acted as a blocking group in **TS-I**. This is an interesting example of a reaction in which one of the groups of the catalyst acts as a sterically hindered substituent in one part of the mechanism and as a directing group in the subsequent part. Hence, this finding highlights the importance of computational mechanistic studies, especially in multi-step reactions since researchers often assume that a specific functional group always plays the same role during the whole reaction.

Therefore, based on the computational results of **TS-II**, the stereoselective-limiting step, if the catalyst does not contain any aromatic group to coordinate with Pd the stereoselectivity obtained should change in a great extent. As expected, modifications of the aromatic ring of the catalyst led to similar enantioselectivities and diastereoselectivity (Scheme 8, (**I**) and (**II**)). In contrast, when the aromatic rings are replaced for aliphatic chains, the stereoselectivity dropped considerably (Scheme 8, (**III**) and (**IV**)). These experimental results are in line with the computational outcomes and support that the aromatic rings are coordinated to Pd during the cyclization step. On the other hand, the reactivity observed with each catalyst is intrinsic to each structure and directly related only with their structure-reactivity profile shown in part 1 of the mechanism (the rate-limiting step).

Finally, to further validate the method by comparing more experimental and theoretical results, we calculated the G of both *syn*- and *anti*-**Int-Ald**, the compound that controls the selectivity of part 1. Experimentally, we observed 38% cinnamaldehyde and 62% **Int-Ald** in the equilibrium at rt, which corresponds to a difference in G (ΔG) of −1.7 kcal mol^{-1} between the G of the initial products and the G of **Int-Ald**. Computationally, the ΔG between diastereomer **Int-Ald** and the initial reagents is −0.4 kcal mol^{-1}, which shows a very low margin of error (1.3 kcal mol^{-1}) in comparison with the experimental result (see *Calculation of the dr in the Equilibrium of Part 1* section in ESI† for more information).

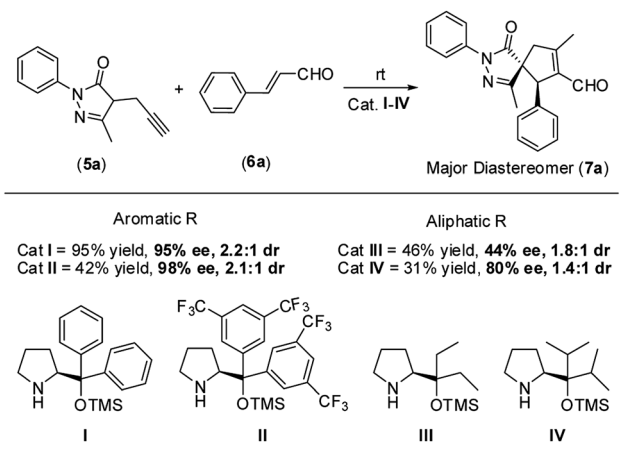

Scheme 8 Experimental results using catalysts I–IV.

Conflicts of interest

There are no conflicts to declare.

Acknowledgements

R. P. H. and J. V. A.-R. thank Ministerio de Economía, Industria y Competitividad (CTQ2017-88091-P) and Gobierno de Aragón Fondo Social Europeo (E07_17R) for funding their research. All calculations were performed at the Trueno cluster facility, SGAI-CSIC. J. V. A.-R. thanks Dr R. Paton for his help with the script to generate the PyMol style and GoodVibes. S. P. and J. V. thank the Czech Science Foundation (No 18-20645S) for funding the study, Dr Hybelbauerová and Dr Tošner for providing the NMR service, Dr Štícha for providing the MS analysis and Dr Carlos V. Melo for proofreading the manuscript. M. M. and R. R. are grateful for EPSRC Core Capability Funding (EP/K039466/1). R. R. thanks Alessandra Carnero for initial studies.

Notes and references

1 R. Rios, *Chem. Soc. Rev.*, 2012, **41**, 1060.
2 D. Cheng, Y. Ishihara, B. Tan and C. F. Barbas III, *ACS Catal.*, 2014, **4**, 743.
3 Z.-Y. Cao and J. Zhou, *Org. Chem. Front.*, 2015, **2**, 849.
4 L.-J. Yan and Y.-C. Wang, *ChemistrySelect*, 2016, **1**, 6948.
5 S. Kotha, N. R. Panguluri and R. Ali, *Eur. J. Org. Chem.*, 2017, 5316.

6 X. Xie, W. Huang, C. Peng and B. Han, *Adv. Synth. Catal.*, 2018, **360**, 194.
7 J. Guang-Mei and F. Shi, *Chem. Commun.*, 2018, **54**, 6607.
8 X. Fang and C.-J. Wang, *Org. Biomol. Chem.*, 2018, **16**, 2591.
9 Y. Zheng, C. M. Tice and S. B. Singh, *Bioorg. Med. Chem. Lett.*, 2014, **24**, 3673.
10 T. L. Pavlovska, R. G. Redkin, V. V. Lipson and D. V. Atamanuk, *Mol. Diversity*, 2016, **20**, 299.
11 P.-Y. Géant, M. Urban, M. Remeš, I. Císařová and J. Veselý, *Eur. J. Org. Chem.*, 2013, 7979.
12 X. Companyó, A. Zea, A.-N. R. Alba, A. Mazzanti, A. Moyano and R. Rios, *Chem. Commun.*, 2010, **46**, 6953.
13 M. Meazza and R. Rios, *Chem.–Eur. J.*, 2016, **22**, 9923.
14 A. E. Allen and D. W. C. MacMillan, *Chem. Sci.*, 2012, **3**, 633.
15 (*a*) M. Meazza and R. Rios, *Synthesis*, 2016, **48**, 960; (*b*) S. Afewerki and A. Cordova, *Chem. Rev.*, 2016, **116**, 13512.
16 G. Varvounis, Pyrazol-3-ones. Part IV: Synthesis and Applications, *Adv. Heterocyclic Chem.*, ed. A. R. Katritzky, Academic Press, 2009, vol. 98, p. 143.
17 P. Chauhan, S. Mahajan and D. Enders, *Chem. Commun.*, 2015, **51**, 12890.
18 V. Hadi, Y. Koh, T. W. Sanchez, D. Barrios, N. Neamati and K. W. Jung, *Bioorg. Med. Chem. Lett.*, 2010, **20**, 6854.
19 Y. L. Janin, *Bioorg. Med. Chem.*, 2007, **15**, 2479.
20 M.-T. Gutierrez-Lugo and C. Bewley, *J. Med. Chem.*, 2008, **51**, 2606.
21 I. R. Matthews, PCT Int. Appl. WO 46679, 2005.
22 A. Kimata, H. Nakagawa, R. Ohyama, T. Fukuuchi, S. Ohta, T. Suzuki and N. Miyata, *J. Med. Chem.*, 2007, **50**, 5053.
23 A. Zea, A.-N. R. Alba, A. Mazzanti, A. Moyano and R. Rios, *Org. Biomol. Chem.*, 2011, **9**, 6519.
24 A. Zea, A.-N. R. Alba, G. Valero, T. Calbet, M. Font-Bardia, A. Moyano and R. Rios, *Eur. J. Org. Chem.*, 2011, 2053.
25 M. Meazza, M. Kamlar, L. Jašíková, B. Formánek, A. Mazzanti, J. Roithová, J. Veselý and R. Rios, *Chem. Sci.*, 2018, **9**, 6368.
26 For an excellent recent review regarding Conia-ene reactions, see: D. Hack, M. Blumel, P. Chauhan, A. R. Phillips and D. Enders, *Chem. Soc. Rev.*, 2015, **44**, 6059.
27 For an example of cooperative catalysis to develop this reaction, see: T. Yang, A. Ferrali, F. Sladojevich, L. Campbell and D. J. Dixon, *J. Am. Chem. Soc.*, 2009, **131**, 9140.
28 (*a*) C. Xu, L. Deiana, S. Afewerki, C. Incerti-Pradillos, O. Cordova, P. Guo, A. Cordova and N. Hedin, *Adv. Synth. Catal.*, 2015, **357**, 2150; (*b*) L. Deiana, Y. Jiang, C. Palo-Nieto, S. Afewerki, C. A. Incerti-Pradillos, O. Verho, C.-W. Tai, E. V. Johnston and A. Cordova, *Angew. Chem., Int. Ed.*, 2014, **53**, 3447.
29 L. Deiana, L. Ghisu, S. Afewerki, O. Verho, E. V. Johnston, N. Hedin, Z. Bacsik and A. Cordova, *Adv. Synth. Catal.*, 2014, **56**, 2485.
30 D. Hack, P. Chauhan, K. Deckers, M. Yusuke, G. Raabe and D. Enders, *Chem. Commun.*, 2015, **51**, 2266.
31 D. Hack, K. Deckers, P. Chauhan, N. Selling, L. Rue-benach, L. Mertens, F. Schoenebeck and D. Enders, *Angew. Chem., Int. Ed.*, 2016, **55**, 1797.
32 M. Meazza, M. E. Light, A. Mazzanti and R. Rios, *Chem. Sci.*, 2016, **7**, 984.
33 M. Meazza, V. Ceban, M. B. Pitak, S. J. Coles and R. Rios, *Chem.–Eur. J.*, 2014, **20**, 16853.
34 V. Ceban, P. Putaj, M. Meazza, M. B. Pitak, S. J. Coles, J. Veselý and R. Rios, *Chem. Commun.*, 2014, **50**, 7447.
35 H. Miyabe and Y. Takemoto, *Bull. Chem. Soc. Jpn.*, 2008, **81**, 785.
36 S. J. Connon, *Chem. Commun.*, 2008, 2499.
37 I. G. Sonsona, E. Marqués-López and R. P. Herrera, *Beilstein J. Org. Chem.*, 2016, **12**, 505.
38 Crystallographic data have been deposited with Cambridge Crystallographic Data Centre: deposit number: CCDC 1859005 and 1859006 for **8b** and **8b′**, respectively.
39 F. Sladojevich, A. L. Fuentes de Arriba, I. Ortín, T. Yang, A. Ferrali, R. S. Paton and D. J. Dixon, *Chem.–Eur. J.*, 2013, **19**, 14286.
40 S. Santoro, L. Deiana, G.-L. Zhao, S. Lin, F. Himo and A. Córdova, *ACS Catal.*, 2014, **4**, 4474 and references therein.
41 For other mechanistic studies using proline (**I**), see also: K. S. Halskov, B. S. Donslund, B. M. Paz and K. A. Jørgensen, *Acc. Chem. Res.*, 2016, **49**, 974.
42 Q. Peng, F. Duarte and R. S. Paton, *Chem. Soc. Rev.*, 2016, **45**, 6093.
43 M. J. Frisch, G. W. Trucks, H. B. Schlegel, G. E. Scuseria, M. A. Robb, J. R. Cheeseman, G. Scalmani, V. Barone, B. Mennucci, G. A. Petersson, H. Nakatsuji, M. Caricato, X. Li, H. P. Hratchian, A. F. Izmaylov, J. Bloino, G. Zheng, J. L. Sonnenberg, M. Hada, M. Ehara, K. Toyota, R. Fukuda, J. Hasegawa, M. Ishida, T. Nakajima, Y. Honda, O. Kitao, H. Nakai, T. Vreven, J. A. Montgomery Jr, J. E. Peralta, F. Ogliaro, M. Bearpark, J. J. Heyd, E. Brothers, K. N. Kudin, V. N. Staroverov, R. Kobayashi, J. Normand, K. Raghavachari, A. Rendell, J. C. Burant, S. S. Iyengar, J. Tomasi, M. Cossi, N. Rega, J. M. Millam, M. Klene, J. E. Knox, J. B. Cross, V. Bakken, C. Adamo, J. Jaramillo, R. Gomperts, R. E. Stratmann, O. Yazyev, A. J. Austin, R. Cammi, C. Pomelli, J. W. Ochterski, R. L. Martin, K. Morokuma, V. G. Zakrzewski, G. A. Voth, P. Salvador, J. J. Dannenberg, S. Dapprich, A. D. Daniels, O. Farkas, J. B. Foresman, J. V. Ortiz, J. Cioslowski and D. J. Fox, *Gaussian 09, Revision D.01*, Gaussian, Inc., Wallingford CT, 2016.
44 A. D. Becke, *J. Chem. Phys.*, 1997, **107**, 8554.
45 J.-D. Chai and M. Head-Gordon, *Phys. Chem. Chem. Phys.*, 2008, **10**, 6615.
46 L. Goerigk and S. A. Grimme, *Phys. Chem. Chem. Phys.*, 2011, **13**, 6670.
47 U. Grošelj, D. Seebach, D. M. Badine, W. B. Schweizer, A. K. Beck, I. Krossing, P. Klose, Y. Hayashi and T. Uchimaru, *Helv. Chim. Acta*, 2009, **92**, 1225.
48 E. Marqués-López and R. P. Herrera, *Curr. Org. Chem.*, 2011, **15**, 2311 and references therein.
49 E. Lyngvi, J. W. Bode and F. A. Schoenebeck, *Chem. Sci.*, 2012, **3**, 2346.
50 K. Świderek, A. R. Nödling, Y.-H. Tsai, L. Y. P. Luk and V. Moliner, *J. Phys. Chem. A*, 2018, **44**, 451.